Theory of the structure factor of lipid bilayers

Ruitian Zhang, Robert M. Suter, and John F. Nagle
Department of Physics, Carnegie Mellon University, Pittsburgh, Pennsylvania 15213
(Received 13 May 1994)

The goal of this research is to obtain the structure of lipid bilayers using low-angle scattering with the **q** vector perpendicular to the bilayers. This requires obtaining the form factor $F(h)$ for the bilayer, which in turn requires correcting the intensity $I(h)$ of the hth order peak by the structure factor $S(q)$, which is a nontrivial function for bilayers in noncrystalline arrays. In this paper the classical theory of smectic liquid crystal scattering is first used to calculate detailed structure factors for unoriented, powder averaged samples. These calculations suggest that the form factors used in conventional biophysical determinations of electron densities require very large corrections. We then show that the classical correlation function in turn requires correction. Our modified correlation function yields much smaller corrections to the form factors. We also modify the standard finite-size factor that is required to fit the peaks. This second modification changes the detailed shape of the peaks while retaining nearly the same form factor corrections and the classical power law tails.

PACS number(s): 87.22.Bt, 87.64.Bx, 61.30.Cz, 61.10.Dp

I. INTRODUCTION

Accurate characterization of the structure of biomembranes is a major interest of the biophysical community [1–20]. This characterization includes the lipid bilayer which forms the basic matrix of the membrane as well as the intrinsic proteins which are responsible for most of the biochemical functionality of membranes. This paper focuses on the lipid bilayer, which ought to be easier to characterize than complex biomembranes, but which continues to pose interesting challenges in biological physics.

The structure of lipid bilayers has been pursued using a number of physical techniques [13–20]. One of the most basic of these is x-ray diffraction [1–12]. A major goal has been to determine electron density profiles along the normal to the bilayers. For phospholipids, the headgroup is electron dense and so determination of the positions of the electron density peaks in such profiles gives a good indication of the thickness of a bilayer [2,8]. Comparison of such thicknesses for bilayers composed of different lipids then gives a database for evaluating the physical effects of different lipids in biomembranes. The widths of the electron density peaks are related to the extent of molecular disorder caused by fluctuations in the bilayer [13,15].

The basic experimental data that have gone into these electron density profiles come from low-angle diffraction from multilamellar arrays. In these arrays the membranes are essentially stacked one upon the other with water layers between, thereby forming a lyotropic smectic liquid crystal. The low-angle scattering consists of fairly sharp peaks that correspond to scattering vectors perpendicular to the bilayers at the values $q_h = 2\pi h/D$ for the different orders h and with the Bragg repeat spacing D that includes the thickness both of one bilayer and of the water between two bilayers. Traditional analyses [4–10] of these data have assumed that the bilayer form factor $F(q)$ (which has sometimes been called the structure factor or structure amplitude) evaluated at q_h is related to the integrated intensity $I(h)$ measured for the hth order peak by

$$I(h) = |F(h)|^2/q_h^2, \tag{1}$$

where $1/q_h^2$ is the usual Lorentz factor. This determines the form factors $F(h)$ (for a particular value of D) except for the phase factor which must be ± 1 for symmetric bilayers; determining phase factors has been the subject of extensive study [4–7] and will not concern us further here. Then, the electron density profile is given by

$$\rho(z) = \sum_h F(h)\cos(2\pi hz/D). \tag{2}$$

The goal of such studies has been to determine the structure of a single bilayer in water, not the structure of bilayers in multilamellar arrays. As in protein crystallography, where it is hoped, and sometimes shown, that the structure of proteins in crystals is very similar to the native structure, it is also hoped that the structure of lipid bilayers determined via Eq. (2) is very similar to that of the single bilayer. This hope seems reasonable when the water space between bilayers is large. Then the continuous form factor is given by

$$F(q) = \int_{-\infty}^{\infty} \rho_I(z)\cos(qz)dz, \tag{3}$$

where $\rho_I(z)$ is the electron density of a single isolated bilayer. If the single bilayer structure is the same as the bilayer structure in multilamellar vesicles, then the discrete form factors $F(h)$ in Eqs. (1) and (2) are the values of $F(q)$ in Eq. (3) evaluated at $q_h = 2\pi h/D$. There is evidence that drying multilamellar arrays eventually changes the quantitative bilayer dimensions by increas-

ing the interlamellar forces [7,8,11]. How much drying is required to change the structure is a matter of some dispute [8,11]; it is hoped that the theory in this paper may help resolve this issue. However, this will be addressed in another paper.

At issue in this paper is whether Eq. (1) is quantitatively accurate for determining the form factors $F(h)$ that are then used in Eq. (2) to obtain the electron density $\rho(z)$ for bilayers in multilamellar arrays. Equation (1) is easily shown to be true when the bilayers are equally spaced in a perfect one-dimensional array along the z axis because then the structure factor $S(q)$ due to the lattice consists of δ functions (Bragg peaks) of equal magnitude for each order h. However, when smectic disorder is included, the classical scattering theory developed by Caillé [21] from the free energy of smectic liquid crystals [22] clearly shows that the $S(q)$ structure factor (often called the interference function) no longer has Bragg peaks but broadened peaks with power law tails. These power law tails have been well established experimentally for a number of smectic systems [23–25] including lipid bilayers [26]. This means that Eq. (1) must be replaced by the more fundamental equation

$$I(q) = S(q)|F(q)|^2, \tag{4}$$

the derivation of which is discussed in the Appendix. It will be convenient to define a reduced structure factor $s(q)$ by explicitly factoring out the usual Lorentz correction. Then, Eq. (4) becomes

$$I(q) = s(q)|F(q)|^2/q^2. \tag{5}$$

Experimentally, the $I(q)$ peaks are narrow enough that there is no difficulty distinguishing the different orders h and the form factor $F(q)$ is practically constant in the narrow region of each of these central peaks. Therefore, if the integrated areas for the hth order peaks of the $S(q)$ and $s(q)$ functions are designated $S(h)$ and $s(h)$, respectively, then to very good approximation $I(h)$ is given by

$$I(h) = S(h)|F(h)|^2 = s(h)|F(h)|^2/q_h^2, \tag{6}$$

where the final equality defines the correction factor $1/s(h)$ that should be applied to $I(h)$ in addition to the Lorentz correction, q_h^2. The question now is whether $s(h)$ for the disordered lattice is nearly constant for the different orders of scattering centered near q_h or whether $s(h)$ significantly varies with h so that the form factors usually calculated from Eq. (1) must be corrected using Eq. (6).

One way to address the question in the preceding paragraph is to use the paracrystalline theory of Hosemann and Bagchi [27]. This is a stochastic non-Hamiltonian theory that only takes into account one of the degrees of freedom relevant for smectic liquid crystals, but it is not as fundamental as the Caillé scattering theory. This question was addressed qualitatively in the context of Caillé theory by Gunther *et al.* [28] when discussing the absence of higher order peaks in liquid crystal data [23]. More recently Nallet *et al.* [29] introduced a kind of hybrid model that looks like the paracrystalline theory, but which uses some aspects of the Caillé correlation function. Nallet *et al.* stated that "it is unfortunately not easy to devise a ... complete rigorous theory" that takes into account all the features of the Caillé theory. We believe that the present paper provides this rigorous development of a quantitative theory that can provide the effective correction factors $1/s(h)$, not only for lipid bilayers, but also for general smectic liquid crystals.

In the next section the classical scattering theory of Caillé and others is briefly reviewed and it is shown that the correction factor $1/s(h)$ can indeed be quite large for values of the parameters indicated from experimental studies. This review shows that there are approximations in the classical theory that need to be addressed before accepting the corrections predicted by the theory as it now exists. Before doing this, however, we turn in Sec. III to describe an accurate approximation that enables us to perform fits to data from powder samples more efficiently as well as to obtain analytic results for theoretical analysis. Then, in Sec. IV we improve the Caillé correlation function which results in considerably different structure factor corrections than the classical theory, as shown by detailed comparisons in Sec. V. In Sec. VI we propose a modification in a different part of the classical theory, due to Dutta and Sinha [30], regarding the finite-size effect on the shape of the scattering peaks. Detailed conclusions are summarized in Sec. VII.

II. CLASSICAL X-RAY SCATTERING THEORY

This section gives a brief review of the classical theory that provides much of the basis for our developments and refinements. Consider a sample consisting of $N+1$ (N even) membranes contained in a cylinder of height L along the z direction and with diameter L_r. On average each membrane is flat with its normal along the z axis of the cylinder, so the average membrane also occupies a cylindrical volume of height $D = L/N$. The structure factor (interference function) for scattering from a smectic liquid crystal sample is given by

$$S(\mathbf{q}) = \sum_{n,m=-N/2}^{N/2} e^{iq_z(n-m)D} \iint_{|\mathbf{r}|,|\mathbf{r}'|\le L_r/2} d^2r d^2r' e^{i\mathbf{q}\cdot(\mathbf{r}-\mathbf{r}')} G(\mathbf{r},\mathbf{r}',n,m), \tag{7}$$

where $G(\mathbf{r},\mathbf{r}',n,m)$ is the scattering pair correlation function for those pieces of membranes numbered n and m whose lateral (in-plane) coordinates are $\mathbf{r}$ and $\mathbf{r}'$, respectively. As suggested by de Gennes [22], the layer displacement u, in the z direction only, sufficiently describes the positional fluctuations of smectic-A liquid crystals. Therefore

$$G(\mathbf{r},\mathbf{r}',n,m) = \langle e^{iq_z[u(\mathbf{r},nD)-u(\mathbf{r}',mD)]}\rangle, \tag{8}$$

where $\langle\ \rangle$ is the thermal average. The pair correlation

function takes into account the fluctuations in the central positions of the membranes. Fluctuations in layer thickness and in molecular conformation are included in the bilayer form factor $F(q)$ (see Appendix). Using the standard harmonic approximation, translational symmetry, and, following Caillé, restricting the scattering vector close to the hth order reflection lead to

$$G(\mathbf{r},z) = e^{-q_h^2\langle[u(\mathbf{r},z)-u(0,0)]^2\rangle/2}. \tag{9}$$

Calculation of $\langle[u(\mathbf{r},z)-u(0,0)]^2\rangle$ in Eq. (9) depends on the free energy of the smectic-A system, which has been given by de Gennes [22] as

$$\frac{F}{V} = \frac{B}{2}\left(\frac{\partial u}{\partial z}\right)^2 + \frac{K}{2}\left(\frac{\partial^2 u}{\partial x^2}+\frac{\partial^2 u}{\partial y^2}\right)^2, \tag{10}$$

where B is the bulk modulus for layer compression and K is the modulus for layer curvature. Following de Gennes [22], the equipartition theorem can be applied to each Fourier component of this free energy. Assuming isotropy in the x-y plane of each bilayer and symmetric bilayers, it is straightforward to show that

$$\langle[u(\mathbf{r},z)-u(0,0)]^2\rangle$$

$$= \frac{4kT}{(2\pi)^2 B}\frac{\pi}{L}\sum_{q_z=0}^{\pi/D}\int_0^{\pi/a}\frac{q_r dq_r\,[1-J_0(q_r r)\cos(q_z z)]}{q_z^2+\lambda^2 q_r^4}, \tag{11}$$

where the upper limit in the in-plane q_r integral is determined by the in-plane spacing a between the lipid molecules, the parameter λ was defined by de Gennes [22] to be $\sqrt{K/B}$, and J_0 is the zeroth order Bessel function. It will be shown that a and λ essentially drop out of our final scattering equations, so it is not critical which values are used for illustration in the figures in this paper. We have chosen $a = 4$ Å, which is close to the acyl chain packing distance; the average distance between lipid molecules with two acyl chains is closer to 6 Å. We have also chosen $\lambda = 12$ Å from measurements of the membrane rigidity $KD \sim 1-2\times10^{-12}$ ergs [31,32] and from Wack and Webb's [26] measurement of $B = 1.9\times10^8$ ergs/cm^3 for fluid phase dilaurylphosphatidylcholine (DLPC).

We have numerically evaluated Eq. (11), and hence the correlation function in Eq. (9), to high accuracy for values of the parameters that we are obtaining from our current experimental data and that are consistent with the values found by others [26,31,32]. An example of this correlation function is shown in Fig. 1 by the curve labeled "precise." In general such calculations are too time consuming for final data analysis and the critical asymptotic behavior is not so obvious, so approximations have been made.

Caillé developed the theory [21] in the limit $L\to\infty$, so he replaced the sum in Eq. (11) by an integral over q_z. He also extended the upper q_z limit of this integral to ∞, which allowed him to obtain a closed form expression in the limit $z \gg a^2/\lambda$,

$$G_C(r,z) = e^{-2\eta_h\gamma}(\pi r/a)^{-2\eta_h}e^{-\eta_h E_1(r^2/4\lambda z)}, \tag{12}$$

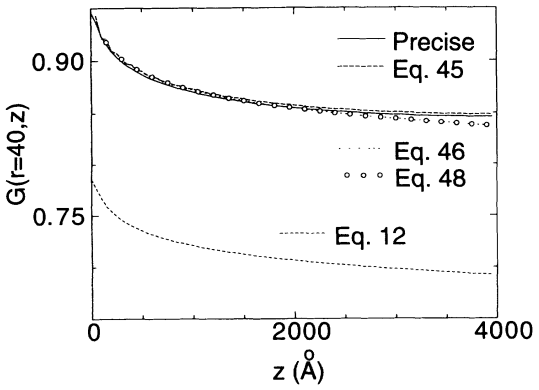

FIG. 1. Numerical calculations of the correlation function $G(r,z)$ versus z for $r = 40$ Å and for $h = 1$, for parameter values $\eta_1 = 0.03$, $D = 60$ Å, $\lambda = 12$ Å, $L = 4000$ Å, $a = 4$ Å. The solid curve labeled "precise" is calculated numerically using Eqs. (9) and (11). The other curves were calculated using various approximations as shown in the figure legend.

where the subscript C denotes the classical theory, E_1 is the exponential integral function, γ is Euler's constant, and η_h are the undulation parameters defined by Caillé as

$$\eta_h = \eta_1 h^2, \tag{13}$$

where

$$\eta_1 = \frac{q_1^2\,kT}{8\pi\sqrt{KB}} = \frac{\pi}{2}\left(\frac{kT}{KD}\frac{kT}{BD^3}\right)^{1/2}. \tag{14}$$

A calculation of $G_C(r,z)$ at $r = 40$ Å is shown in Fig. 1 for the same set of parameters as those used for the calculation of the precise correlation function. The main reason for the discrepancy comes from replacing the finite q_z cutoff π/D by ∞ in Eq. (11). Despite this discrepancy, the main results of Caillé regarding the asymptotic behavior of the correlation function and the power law tails of the scattering peaks remain intact. This discrepancy does, however, affect the relative magnitudes of the $s(h)$ factors in Eq. (6), which is the focus of this paper.

The final piece of the classical theory involves the recognition that samples consist of domains with finite sizes, but that not all the domains will have precisely the same size. Generally, the structure factor $S(\mathbf{q})$ for $(0,0,h)$ peaks of oriented samples can be written as [33]

$$S(\mathbf{q}) = \int_{-\infty}^{\infty} d^3R\; H(\mathbf{R})G(\mathbf{R})e^{i(\mathbf{q}-q_h\hat{\mathbf{z}})\cdot\mathbf{R}}, \tag{15}$$

where the factor $H(\mathbf{R})$ in the integrand is the finite-size factor, and where for layered systems it is appropriate to use

$$\mathbf{R} = \mathbf{r} + z\hat{\mathbf{z}}. \tag{16}$$

Dutta and Sinha [30] proposed a one-parameter theory involving a coherence length L that represents the average size of domains in the sample. Following the ideas of Dutta and Sinha yields for $H(\mathbf{r},z)$ the function [24,25]

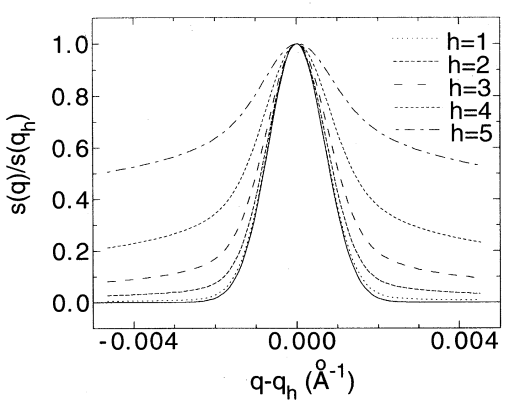

FIG. 2. Normalized reduced structure factor $s(q)/s(q_h)$ versus $q-q_h$ calculated from the classical formulas Eqs. (12), (17), (18), and (5) for parameters $D = 60$ Å, $\lambda = 12$ Å, $a = 4$ Å, and $L = 4000$ Å. The solid curve shows the peak for the nonfluctuating case ($\eta = 0$) for comparison. The other curves show the first five orders for $\eta_1 = 0.03$. The correction factors $1/s(q_h)$ have the values 1.41, 4.17, 20.4, 189, 2442 for $h = 1, \ldots, 5$, respectively.

$$H_C(\mathbf{r}, z) = e^{-\pi(r^2+z^2)/L^2}, \tag{17}$$

where the C subscript again designates classical.

Equations (12) and (17) are the basic formulas from the classical theory that are used to compute the structure factor in the fundamental Eq. (15). When this is applied to powder samples [24,25], the structure factor may be written in the form

$$S(q) = \int_{-\infty}^{\infty} d^3R\, H(\mathbf{R})G(\mathbf{R})e^{-iq_h z}\, \frac{\sin\, q\sqrt{r^2+z^2}}{q\sqrt{r^2+z^2}}. \tag{18}$$

Figure 2 shows calculations for the reduced structure factors $s(q)$ using Eqs. (12), (17), (18), and (5). This figure clearly shows the well-known result that the power law tails become more pronounced for the higher orders h of reflection due to the quadratic dependence of the undulation parameters η_h on h.

More important for our study is the dramatic effect of smectic fluctuations on the peak intensity, $s(q_h)$. In Fig. 2 the $s(q)$ curves have been normalized to 1 at $q = q_h$ for all orders h. If there were no fluctuations, then the factors $s(q_h)$ would all equal one. As shown in the caption to Fig. 2, however, the normalization factors $1/s(q_h)$ increase strongly with h. In Sec. VI we will consider the issue of increases in the peak widths with h and how this affects $I(h)$ with power law tails. Here let us only remark that, when $I(h)$ is measured in the usual way, the increased width is a minor effect compared to the decrease in the height $s(q_h)$ with h. Then, the correction factors $1/s(h)$ are numerically similar to the normalization factors $1/s(q_h)$, so the large increase in $1/s(q_h)$ for the higher orders in Fig. 2 suggests that neglect of fluctuations would contribute a large error in determining form factors for bilayer structure using Eq. (1). Since these corrections are so large, it is important that the theory be carefully examined to see whether such corrections are quantitatively accurate, especially when the results in Fig. 1 indicate that the Caillé correlation functions are quantitatively inaccurate. This motivates our proposed modifications.

III. APPROXIMATE POWDER AVERAGE FORMULA

We will first develop an approximate method for calculating powder averages in this section. This is an essential approximation that is key to our other theoretical developments, as well as to performing numerical fits to data.

We start from Warren's powder pattern power theorem [34] of x-ray scattering which simply states that the scattering power P from a powder sample is

$$P \propto \frac{1}{4\pi}\iiint dq_x dq_y dq_z S(q_x, q_y, q_z)/q = \int dq\; qS(q), \tag{19}$$

where $q = \sqrt{q_x^2+q_y^2+q_z^2}$ and the $1/q$ factor is from the powder diffraction geometry. Changing the variable set $(q_x, q_y, q_z) \rightarrow (q_x, q_y, q)$ for $q_z > 0$ and $(q_x, q_y, q_z) \rightarrow (q_x, q_y, -q)$ for $q_z < 0$ yields

$$dq_x dq_y |dq_z| = dq_x dq_y \frac{q}{\sqrt{q^2-q_x^2-q_y^2}} dq. \tag{20}$$

Substituting Eq. (20) into (19), and eliminating the integral over q on both sides, the expression for $S(q)$ in Eq. (19) becomes

$$S(q) = \iint_{q_x^2+q_y^2 \le q^2} dq_x dq_y \frac{S(q_x, q_y, \sqrt{q^2-q_x^2-q_y^2}) + S(q_x, q_y, -\sqrt{q^2-q_x^2-q_y^2})}{4\pi q\sqrt{q^2-q_x^2-q_y^2}}. \tag{21}$$

Substituting the integral form of the structure factor $S(\mathbf{q})$ from Eq. (15) into Eq. (21) yields

$$S(q) = \frac{1}{4\pi q}\int_{-\infty}^{\infty} d^3R\, H(\mathbf{R})G(\mathbf{R})e^{-iq_h z} \iint_{q_x^2+q_y^2 \le q^2} dq_x dq_y\, \frac{e^{iq_x x+q_y y}\cos(\sqrt{q^2-q_x^2-q_y^2}z)}{\sqrt{q^2-q_x^2-q_y^2}}. \tag{22}$$

Letting $q_r = \sqrt{q_x^2 + q_y^2}$, one obtains

$$S(q) = \frac{1}{q}\int d^3R\, H(\mathbf{R})G(\mathbf{R})e^{-iq_h z} \times \int_0^q dq_r \frac{q_r J_0(q_r r)\cos(\sqrt{q^2 - q_r^2}\,z)}{\sqrt{q^2 - q_r^2}}. \quad (23)$$

Equation (23) is still exactly equivalent to Eq. (18).

Equation (23) is by no means simpler than Eq. (18); on the contrary, it is more complicated. However, Eq. (23) is amenable to a useful approximation. To see this, we notice that for relatively large scattering systems, the $(0,0,h)$ peaks are fairly sharp. This means that $q_h \sim q \gg q_r$ for $h \neq 0$, so it is reasonable to consider the approximation

$$\sqrt{q^2 - q_r^2} \approx q\ , \quad (24)$$

in the cosine function in Eq. (23). Then, I_q, the integral over q_r in Eq. (23), can be evaluated using Eq. 24 to yield

$$I_q \approx \cos(qz)\int_0^q dq_r\, \frac{q_r J_0(q_r r)}{\sqrt{q^2 - q_r^2}} = \cos(qz)\frac{\sin(qr)}{r}. \quad (25)$$

Therefore Eq. (23) is simplified to

$$S(q) = \int_{-\infty}^{\infty} d^3R\, H(\mathbf{R})G(\mathbf{R})e^{-iq_h z}\cos(qz)\frac{\sin(qr)}{qr}. \quad (26)$$

The difference between Eq. (26) and Eq. (18) is the factorization of the r dependence from the z dependence in the phase factors.

To investigate the accuracy of Eq. (26), we calculate $S(q)$ from both Eq. (26) and Eq. (18) for the same set of parameters as in Fig. (2), and display the two results in Fig. 3. The approximate result from Eq. (26) matches the precise result quite well. The relative errors are generally very small (~1%) for most of the q values, although in the tail region near the ends of the curves shown in Fig. 3 the relative errors are as large as 10%. Nevertheless, the absolute errors are much smaller than typical experimental errors. The basic difference is due to the fact that the approximation is almost symmetrical about q_h whereas the exact equation (18) has a slight asymmetry with larger values for $q > q_h$ than for $q < q_h$.

To test the accuracy of Eq. (26) further, we next examine a case that can be calculated exactly, namely, the case of nonfluctuating bilayers, $G(\mathbf{R}) \equiv 1$, and $H(\mathbf{R}) = e^{-\pi(r^2+z^2)/L^2}$. The exact calculation from Eq. (18) yields

$$S(q) = \frac{\pi L}{qq_h}\left(e^{-L^2(q-q_h)^2/4\pi} - e^{-L^2(q+q_h)^2/4\pi}\right), \quad (27)$$

as shown by Roux and Safinya [25]. For this same case, Eq. (26) yields

$$S(q) = \frac{\pi L}{q^2}\left(e^{-\frac{L^2(q-q_h)^2}{4\pi}} + e^{-\frac{L^2(q+q_h)^2}{4\pi}}\right)\frac{L^2q^2}{2\pi} \times {}_1F_1\left(1, \frac{3}{2}, \frac{-L^2q^2}{4\pi}\right), \quad (28)$$

where the ${}_1F_1$ function is the degenerate hypergeometric function. Figure 4 shows the structure factors $S(q)$ calculated from Eq. (27) and Eq. (28), respectively: the two curves differ by less than 0.1% in the range over which the intensities decay four orders of magnitude.

Now that we have established the numerical accuracy of Eq. (26), we can utilize the factorization of the r dependent and z dependent phase factors. In particular, the factor $\sin(qr)$ shows that the integral in the x-y plane is very oscillatory. This suggests that the contributions from the large r region to the $S(q)$ integral are much smaller than those from the small r region. In other words, the $S(q)$ integral is very insensitive to the value of the integrand at large r. Therefore, when we calculate the correlation function $G(r,z)$ and finite-size factor $H(\mathbf{R})$ in the following sections, it will be possible to use expansions in r.

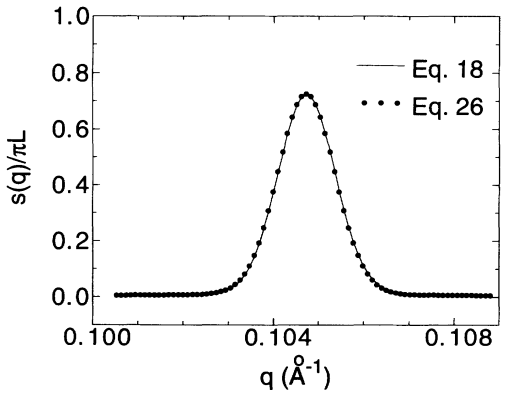

FIG. 3. Comparison of the reduced structure factors $s(q)/\pi L$ versus q calculated from Eqs. (18) (solid line) and (26) (solid circles) for the first order ($h = 1$) peak for parameter values $\eta_1 = 0.03$, $L = 4000$ Å, $D = 60$ Å, $\lambda = 12$ Å, $a = 4$ Å.

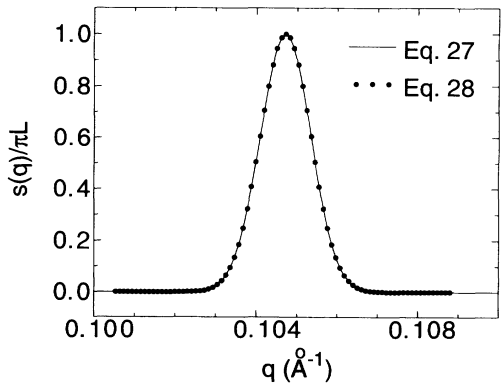

FIG. 4. Comparison of the reduced structure factors $s(q)/\pi L$ versus q calculated from Eq. (27) (solid line) and Eq. (28) (solid circles) for parameter values $L = 4000$ Å, $D = 60$ Å, and $\eta_1 = 0$.

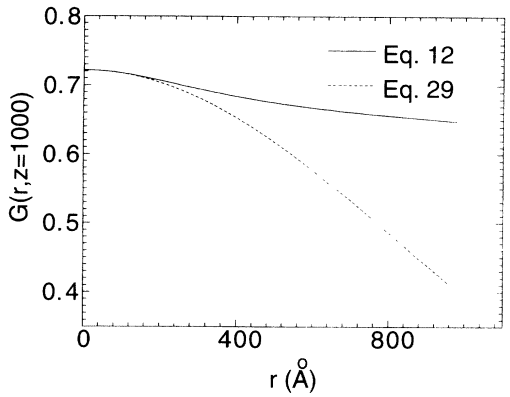

FIG. 5. Comparison of the r dependence of the correlation functions for $z = 1000$ Å from Eq. (29) (dashed line) and Eq. (12) (solid line) for the first order ($h = 1$) peak for parameter values $\eta_1 = 0.03$, $L = 4000$ Å, $D = 60$ Å, $\lambda = 12$ Å, and $a = 4$ Å.

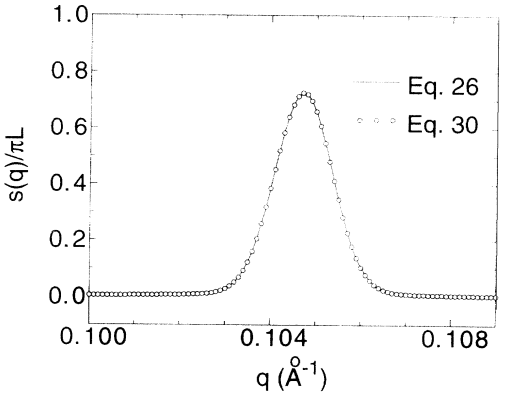

FIG. 6. Comparison of the reduced structure factors $s(q)/\pi L$ versus q calculated from Eq. (26) (solid line) and Eq. (30) (circles) for the first order peak ($h = 1$) for parameter values $\eta_1 = 0.03$, $L = 4000$ Å, $D = 60$ Å, $\lambda = 12$ Å, and $a = 4$ Å.

To demonstrate the point argued in the preceding paragraph, we approximate the classical correlation function $G_C(r,z)$ in Eq. (12) by expanding the E_1 function in Eq. (12) with respect to r to obtain

$$G_C(r,z) \approx G_C(0,z)e^{-\eta_h r^2/4\lambda z} = e^{-\eta_h \gamma}\left(\frac{4\pi^2\lambda z}{a^2}\right)^{-\eta_h} e^{-\eta_h r^2/4\lambda z}, \quad z \neq 0. \tag{29}$$

The r dependence of this approximation is compared in Fig. 5 to the exact r dependence from Eq. (12). Next, let us examine the effect of using the expansion in Eq. (29) for the calculation of $S(q)$. Using Eq. (29) and the classical finite-size factor $H(\mathbf{R})$ from Eq. (17) in Eq. (26) yields

$$S(q) = \frac{4\pi}{q}\int_0^\infty dz\, G_C(0,z)e^{-\pi z^2/L^2}e^{-iq_h z}\cos(qz) \times \int_0^\infty dr\, e^{-\eta_h r^2/4\lambda z}e^{-\pi r^2/L^2}\sin(qr). \tag{30}$$

We have calculated $S(q)$ using both Eq. (26) and Eq. (30), and plotted the two results in Fig. 6. Despite the inaccuracy of the approximation for the correlation function shown in Fig. 5, the two results for $S(q)$ match almost perfectly.

In the preceding paragraph we have shown that, for the calculation of $S(q)$ using Eq. (26) and for the case of a classical correlation function $G_C(r,z)$, it is accurate enough to expand with respect to r, and only keep terms up to r^2. We note that this is mostly due to the oscillatory phase factor $\sin(qr)$, not because of the particular functional form of $G_C(r,z)$. Therefore we anticipate that the above conclusion should hold for more general cases, that is, for any correlation function $G(r,z)$ which can be written in the form

$$G(r,z) = e^{-g(r,z)}, \tag{31}$$

where $g(r,z)$ can be expanded as

$$g(r,z) = g_0(z) + g_1(z)r^2 + O(r^4) > 0, \tag{32}$$

provided

$$g_1(z) \ll \frac{1}{D^2} \tag{33}$$

is true for most of the z values. Therefore the correlation function $G(r,z)$ can be approximated by

$$G(r,z) \approx e^{-g_0(z)}e^{-g_1(z)r^2}, \tag{34}$$

for the calculation of $S(q)$, provided the conditions in Eqs. (32) and (33) hold.

IV. REFINED CORRELATION FUNCTION FOR FINITE-SIZE SAMPLES

To calculate the scattering correlation function for finite-size samples, we start from the general formula in Eq. (11), rather than just follow Caillé. Replacing q_z by $n\pi/L$ and defining $\Delta U(r,z)$, we write out the sum in Eq. (11) explicitly as

$$\Delta U(r,z) \equiv \langle[u(r,z) - u(0,0)]^2\rangle = \frac{4kT}{(2\pi)^2 B}\frac{\pi}{L} \times \sum_{n=0}^{N}\int_0^{\pi/a}\frac{q_r dq_r[1 - J_0(q_r r)\cos(n\pi z/L)]}{(n\pi/L)^2 + \lambda^2 q_r^4}. \tag{35}$$

Equation (35) is too complicated to express by closed form analytical functions; it is also very time consuming for numerical calculations. Therefore proper approximations should be considered.

In order to put the correlation function $G(r,z)$ into the form of Eq. (34), we expand the Bessel function J_0 in Eq. (35) to order r^2 to obtain the approximation

$$\Delta U(r,z) \approx \frac{4kT}{(2\pi)^2 B}\frac{\pi}{L}\sum_{n=0}^{N}\int_0^{\pi/a}\frac{q_r dq_r\{1-[1-(q_r r)^2/4]\cos(n\pi z/L)\}}{(\frac{n\pi}{L})^2+\lambda^2 q_r^4}. \tag{36}$$

We separate ΔU into two parts:

$$\Delta U = \Delta U_1 + \Delta U_2\ , \tag{37}$$

where

$$\Delta U_1 = \Delta U(0,z) = \frac{4kT}{(2\pi)^2 B}\frac{\pi}{L}\sum_{n=0}^{N}\int_0^{\pi/a}\frac{q_r dq_r\,[1-\cos(n\pi z/L)]}{(n\pi/L)^2+\lambda^2 q_r^4}, \tag{38}$$

and

$$\Delta U_2 = \Delta U(r,z) - \Delta U(0,z) = \frac{r^2 kT}{(2\pi)^2 B}\frac{\pi}{L}\sum_{n=0}^{N}\int_0^{\pi/a}\frac{dq_r q_r^3\cos(n\pi z/L)}{(n\pi/L)^2+\lambda^2 q_r^4}. \tag{39}$$

Evaluation of the q_r integral in Eq. (38) yields

$$\Delta U_1 = \frac{4kT}{(2\pi)^2 B}\frac{1}{2\lambda}\sum_{n=0}^{N}\frac{1-\cos(n\pi z/L)}{n}\tan^{-1}\left(\frac{\lambda\pi L}{na^2}\right). \tag{40}$$

Since $\lambda\pi L/na^2 = (\lambda\pi D/a^2)(N/n) \gg 1$, we can set $\tan^{-1}(\lambda\pi L/na^2) \approx \pi/2$, and obtain

$$\Delta U_1 = \frac{4kT}{(2\pi)^2 B}\frac{\pi}{4\lambda}\sum_{n=0}^{N}\frac{1-\cos(n\pi z/L)}{n} = \frac{2\eta_1}{q_1^2}\sum_{n=0}^{N}\frac{1-\cos(n\pi z/L)}{n}. \tag{41}$$

For small r, $\Delta U_2(r,z)$ in Eq. (39) is small. Because the integrand goes asymptotically as q_z^{-2} in q_z and goes as q_r^{-1} in q_r, we replace the sum by an integral from 0 to ∞, and obtain

$$\Delta U_2(r,z) \approx \frac{r^2 kT}{(2\pi)^2 B}\int_0^{\infty} dq_z\int_0^{\pi/a}\frac{dq_r q_r^3\cos(q_z z)}{q_z^2+\lambda^2 q_r^4} = \frac{kT}{(2\pi)^2 B}\frac{\pi}{\lambda}\frac{r^2}{4\lambda z}\left(1-e^{-\lambda z\pi^2/a^2}\right). \tag{42}$$

Since $\lambda z\pi^2/a^2 \gg 1$ for $z > D$, we obtain

$$\Delta U_2(r,z) \approx \frac{kT}{(2\pi)^2 B}\frac{\pi}{\lambda}\frac{r^2}{4\lambda z}. \tag{43}$$

Therefore, for $r^2 < 4\lambda z$, and $z \neq 0$, we obtain the approximation, designated by the subscript $A1$,

$$\langle[u(r,z)-u(0,0)]^2\rangle_{A1} = \frac{2\eta_1}{q_1^2}\left(\sum_{n=0}^{N}\frac{1-\cos(n\pi z/L)}{n}+\frac{r^2}{4\lambda z}\right). \tag{44}$$

The corresponding correlation function G_{A1} is

$$G_{A1}(r,z) = \exp\left(-\eta_h\sum_{n=0}^{N}\frac{1-\cos(n\pi z/L)}{n}\right)e^{-\frac{\eta_h r^2}{4\lambda z}}. \tag{45}$$

Now, we can check the validity condition in Eq. (33) for $G_{A1}(r,z)$. Here, we have $g_1(z) = \eta_h/(4\lambda z)$. It is obvious that $g_1(z) \ll 1/D^2$ for $z \gg D$. Therefore $G_{A1}(r,z)$ will be sufficient for the calculation of $S(q)$. When $N = L/D$ is large, the sum in Eq. (45) can be replaced by an integral, and thus the correlation function can be written in a closed form which we call G_{A2}:

$$G_{A2}(r,z) = e^{-\eta_h \mathrm{Cin}(\pi z/D)}e^{-\frac{\eta_h r^2}{4\lambda z}}, \tag{46}$$

where $\mathrm{Cin}(x) = \int_0^x dt(1-\cos t)/t$ is the cosine integral function.

The accuracy of our approximate correlation functions is shown in Fig. 1. The correlation function G_{A1} from Eq. (45) is fairly close to the exact correlation function, with relative errors of about 2%. One point worth noticing is that both the precise correlation function and G_{A1} from Eq. (45) decay more and more slowly as $z \to L$, and become flat at $z = L$. The correlation function G_{A2} from Eq. (46) is also rather close to the precise correlation function. It, however, decays algebraically for all large z, as a result of the infinite-size approximation.

An analytic comparison to the Caillé correlation function G_C in Eq. (12) can now be made. The asymptotic expansion for z/D large,

$$\mathrm{Cin}(\pi z/D) \sim \gamma + \ln(\pi z/D), \tag{47}$$

can be employed in Eq. (46) to yield

$$G_{A2}(r,z) \approx G_{A3} = e^{-\eta_h\gamma}(\pi z/D)^{-\eta_h}e^{-\eta_h r^2/4\lambda z}. \tag{48}$$

For comparison with other correlation functions, $G_{A3}(r,z)$ is calculated using the same set of parameters as our previous calculations, and plotted in Fig. 1. Clearly, $G_{A3}(r,z)$ from Eq. (48) is nearly identical to G_{A2} from Eq. (46), which suggests that the expansion in Eq. (47) is very accurate. For large z and small r, G_C in Eq. (12) yields

$$G_C(r,z) \approx e^{-\eta_h\gamma}(4\pi\lambda z/a^2)^{-\eta_h}e^{-\eta_h r^2/4\lambda z}. \tag{49}$$

It can now be seen analytically that the Caillé correlation function is too small by using Eq. (49) and Eq. (48) to calculate the ratio

$$\frac{G_{A3}}{G_C} = \left(\frac{4\pi\lambda D}{a^2}\right)^{\eta_h} > 1. \tag{50}$$

This ratio is greater than 1 for lipid bilayers because D (of order 60 Å) and λ (of order 12 Å) are greater than a (of order 4 Å) and η_h is intrinsically positive. This shows

that the classical correlation function G_C underestimates the degree of order in smectic liquid crystal systems.

V. ANALYTICAL RESULTS USING THE CLASSICAL FINITE-SIZE FACTOR

Although another form of the finite-size factor will be proposed in the next section, we wish first to discuss the structure factor $S(q)$ using the classical finite-size factor in Eq. (17). Although we believe that these expressions are not the best for data fitting, they are illuminating in semiquantitative discussions because closed form expressions for $S(q)$ from Eq. (26) can be obtained.

Let us write the correlation function G_{A3} in Eq. (48) as

$$G_{A3}(r,z) = G_{A3}(0,D)(z/D)^{-\eta_h} e^{-\eta_h r^2/4\lambda z}, \tag{51}$$

where $G_{A3}(0,D) = (\pi e^{\gamma})^{-\eta_h}$ is the correlation function at the position $(0,D)$. Then, combining Eqs. (17), (26), and (51), we obtain

$$S(q) = \frac{4\pi G_{A3}(0,D)}{qD^{-\eta_h}} \int_0^\infty dz\; z^{-\eta_h} e^{-\pi \frac{z^2}{L^2}} \cos(q_h z)\cos(qz) \times \int_0^\infty dr\; e^{-\frac{\eta_h r^2}{4\lambda z}} e^{-\pi \frac{r^2}{L^2}} \sin(qr). \tag{52}$$

Defining $\Lambda = \eta_h/4\lambda z + \pi/L^2$, we obtain

$$S(q) = \frac{2\pi G_{A3}(0,D)}{D^{-\eta_h}} \int_0^\infty dz\; z^{-\eta_h+1} e^{-\pi z^2/L^2} \cos(q_h z) \times \cos(qz)\; {}_1F_1\left(1, \frac{3}{2}, \frac{-q^2}{4\Lambda}\right)\Big/\Lambda. \tag{53}$$

Since $q^2/4\Lambda = q^2/(\eta_h/\lambda z + 4\pi/L^2) > 1$ for $z > D$, we perform an asymptotic expansion of the ${}_1F_1$ function,

$${}_1F_1\left(1, \frac{3}{2}, \frac{-q^2}{4\Lambda}\right) \sim \frac{1}{2}\left(\frac{q^2}{4\Lambda}\right)^{-1}. \tag{54}$$

Then, Eq. (53) yields

$$S(q) = \frac{4\pi G_{A3}(0,D)}{q^2 D^{-\eta_h}} \int_0^\infty dz\; z^{-\eta_h} e^{-\pi z^2/L^2} \cos(q_h z)\cos(qz). \tag{55}$$

Using the standard integral formula, we evaluate Eq. (55) and obtain the following closed form:

$$S(q) = S_t(q) + S_m(q), \tag{56}$$

where

$$S_t(q) = \left[\frac{\pi^{(1+\eta_h)/2} G_{A3}(0,D) L}{q^2} \Gamma\left(\frac{1-\eta_h}{2}\right)\left(\frac{L}{D}\right)^{-\eta_h}\right] \times {}_1F_1\left(\frac{1-\eta_h}{2}, \frac{1}{2}, \frac{-L^2(q-q_h)^2}{4\pi}\right), \tag{57}$$

and

$$S_m(q) = \left[\frac{\pi^{(1+\eta_h)/2} G_{A3}(0,D) L}{q^2} \Gamma\left(\frac{1-\eta_h}{2}\right)\left(\frac{L}{D}\right)^{-\eta_h}\right] \times {}_1F_1\left(\frac{1-\eta_h}{2}, \frac{1}{2}, \frac{-L^2(q+q_h)^2}{4\pi}\right). \tag{58}$$

$S_t(q)$ is the standard "true" hth order peak. The "mirror" peak centered at $q = -q_h$, $S_m(q)$, is extremely small for positive q and thus can be neglected. For numerical calculations we use the more accurate correlation function G_{A2} in Eq. (46), instead of G_{A3}, in order to avoid the weak divergence at $z = 0$. In parallel with the above derivation, we obtain

$$S(q) = \frac{4\pi}{q^2} \int_0^\infty dz\; e^{-\eta_h \mathrm{Cin}(\pi z/D)} e^{-\pi z^2/L^2} \cos(q_h z)\cos(qz). \tag{59}$$

Figure 7 shows five harmonic peaks using Eq. (59) and the same values of the parameters L, D, and η_h as in Fig. 2. It is noteworthy that the other parameters, a and λ, that were required for Fig. 2, do not appear in Eq. (59). The a parameter played only a minor role, as would be expected, in the correlation function, and this role was eliminated with little error in the G_{A1} approximation developed in Sec. IV. The λ parameter is associated with the r dependence. The general development in Sec. III shows that the structure is rather insensitive to the r dependence and the development in the preceding paragraph supports this by the disappearance of the λ parameter.

The shape of the peaks in Eq. (57) is determined by the ${}_1F_1$ function because it has the only $(q-q_h)$ dependence. By expanding the ${}_1F_1$ function with respect to $(q-q_h)$ for small $(q-q_h)$, one sees that the top of the peak is Gaussian-like:

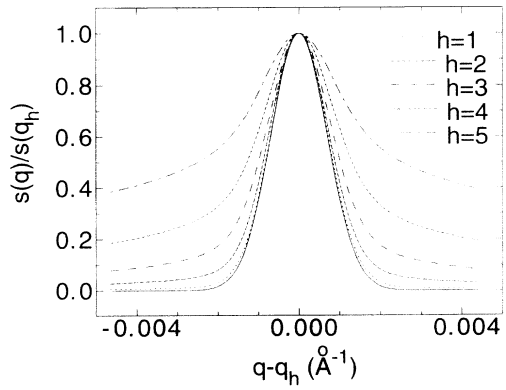

FIG. 7. Normalized reduced structure factor $s(q)/s(q_h)$, calculated from Eq. (59), for parameters $D = 60$ Å, and $L = 4000$ Å. The solid curve shows the peak for the nonfluctuating case ($\eta = 0$) for comparison. The other curves show the first five orders for $\eta_1 = 0.03$. The correction factors $1/s(q_h)$ have the values 1.14, 1.67, 3.09, 6.78, 15.8 for $h = 1, \ldots, 5$, respectively.

$$S(q) \propto 1 - \frac{(1-\eta_h)L^2(q-q_h)^2}{4\pi} \approx e^{-(1-\eta_h)L^2(q-q_h)^2/4\pi}. \tag{60}$$

For $|q - q_h| \gg 1/L$ the tails of the peak decay algebraically:

$$S(q) \propto |q - q_h|^{-1+\eta_h}. \tag{61}$$

Notice that, as a result of powder averaging, the structure factor $S(q)$ in Eq. (61) decays more slowly than the well-known Caillé structure factor for oriented samples. Although the additional macroscopic disorder introduced by powder samples retains algebraic decay of the peak tails, it does change the exponents from $-2+\eta_h$ for oriented samples to $-1+\eta_h$ for powder averaged samples. This $-1+\eta_h$ decay exponent was discovered experimentally [24,25], and was discussed theoretically [33].

Now, let us examine the peak heights $s(q_h)$ as a function of h. In Eq. (57), the factor in the large square brackets determines the peak height dependence on h, since ${}_1F_1{=}1$ at $q = q_h$. The factor $1/q^2$ is the usual Lorentz factor. The peak heights are further reduced, mostly by the factor $(L/D)^{-\eta_h}$. This factor is clearly a result of cooperative thermal fluctuations because it depends strongly on $N = L/D$. This latter property is quite distinct from the usual Debye-Waller factor, as is the change in the shape of the peaks. There is also a factor $G_{A3}(0,D) = (\pi e^{\gamma})^{-\eta_h}$, which describes the positional correlation between two adjacent bilayers, which is rather similar to the Debye-Waller factor [21,34].

Detailed comparison of Fig. 7 to Fig. 2, in which the same values of the basic parameters were used, shows that the shapes of the corresponding peaks are very similar. However, the peak heights $s(q_h)$ in Fig. 2 decrease much more rapidly as a function of h than those in Fig. 7. This dramatic difference can be understood by recalling that the classical correlation function $G_C(r,z)$ [Eq. (12)] was used in the calculations for Fig. 2, while the correlation function $G_{A2}(r,z)$ [Eq. (46)] was used for Fig. 7. Following the methodology of calculating $S(q)$ in Sec. III, only the asymptotic form of $G_C(r,z)$ in Eq. (49) is necessary for the calculations of $S(q)$ in Fig. 2. As we discussed in Sec. IV, and showed in Eq. (50), the ratio of these two correlation functions is $G_{A3}/G_C = (4\pi\lambda D/a^2)^{\eta_h}$, which numerically is 565^{η_h} for the given set of parameters. This numerical factor is basically the ratio of the peak heights $s(q_h)$ in Fig. 7 and Fig. 2. This comparison shows that the modification of the correlation function presented in Sec. IV has considerable numerical consequences for the correction factors $1/s(h)$.

VI. NEW FINITE-SIZE FACTOR

The simplest way to obtain a finite-size factor is to suppose that all the domains have the same size and shape [34,35]. As is well known, this choice predicts oscillations in the tails of the structure factors which are seldom observed experimentally. Dutta and Sinha [30] proposed that Warren's approximation [36] takes into account "the 'smearing' due to superposition of many different domains." This yields the classical finite-size factor in Eq. (17). It should be noted, however, that this finite-size factor has only one parameter L, which represents the average domain size, so it is unclear how the average is done. In contrast to these two methods, we propose another method, which is partially inspired by Ref. [33]. We start from a single sharply edged domain, and then use a size distribution function to perform a size average. Increasing the width of the distribution function eliminates the oscillations in the tails of the structure factor.

A. Finite-size factor for a single size domain

In this subsection we calculate the finite-size factor $H(\mathbf{R})$ for a single sharply edged domain, which consists of $N+1$ membranes of size $L_x \times L_y$. Since $H(\mathbf{R})$ should not depend upon fluctuations, it is convenient to consider the electron density function for a domain of nonfluctuating sheets,

$$\rho_d(x,y,z) = \Theta(L_x/2 - |x|)\Theta(L_y/2 - |y|) \times \sum_{n=-N/2}^{N/2} \delta(z - nD), \tag{62}$$

where Θ is the Heaviside step function. The corresponding structure factor will be written $S_0(\mathbf{q})$. As is well known, $S_0(\mathbf{q})$ for the $(0,0,h)$ peak is given by

$$S_0(\mathbf{q}) = \left| \int d^3R\ \rho_d(\mathbf{R}) e^{i(\mathbf{q}-\mathbf{q}_h)\cdot\mathbf{R}} \right|^2 = \left(\frac{\sin[N(q_z - q_h)D/2]}{\sin[(q_z - q_h)D/2]} \frac{\sin(L_x q_x/2)}{q_x} \frac{\sin(L_y q_y/2)}{q_y} \right)^2. \tag{63}$$

It was Warren [36] who suggested approximating structure factors such as the one in Eq. (63) by Gaussians with the same integrated intensity. However, following [33] we emphasize that there is a fundamental difference between a Gaussian peak and Eq. (63). The tails of Eq. (63) are, of course, dominated by oscillations, but these will disappear when a suitable distribution of domain sizes is employed in Sec. VI C. It is therefore appropriate to consider the amplitude of these oscillations; these only decay as $1/(\delta q)^2$ in Eq. (63). Therefore the tails in Eq. (63) are fundamentally different from Gaussians, which decay very rapidly as $e^{-(\delta q L)^2/4\pi}$.

Using Warren's approximation, Dutta and Sinha obtained the classical finite-size factor $H_C(\mathbf{R})$ in Eq. (17). This specific result follows by considering the general Eq. (15) when $G(\mathbf{R}) = 1$,

$$S_0(\mathbf{q}) = \int d^3R\ H(\mathbf{R}) e^{i(\mathbf{q}-\mathbf{q}_h)\cdot\mathbf{R}}. \tag{64}$$

The finite-size factor may then generally be obtained by Fourier transform,

$$H(\mathbf{R}) = \frac{1}{(2\pi)^3}\int d^3q\; S_0(\mathbf{q})e^{-i(\mathbf{q}-\mathbf{q}_h)\cdot\mathbf{R}}. \tag{65}$$

Using Eq. (65), Eq. (63), and the Fourier folding theorem, the exact $H(\mathbf{R})$ can be expressed as the convolution

$$H(\mathbf{R}) = \rho_d(\mathbf{R}) * \rho_d(-\mathbf{R}). \tag{66}$$

For the finite-size domain in Eq. (62), Eq. (66) yields

$$H(\mathbf{R}) = D\sum_{n=-N}^{N}(N-|n|)\delta(z-nD)\;(L_x-|x|) \times\Theta(L_x-|x|)(L_y-|y|)\Theta(L_y-|y|). \tag{67}$$

In the continuum approximation $nD \to z$, this becomes (using $L = ND$)

$$H(\mathbf{R}) = (L-|z|)\Theta(L-|z|)(L_x-|x|)\Theta(L_x-|x|) \times(L_y-|y|)\Theta(L_y-|y|). \tag{68}$$

Figure 8 compares the z variation of $H(\mathbf{R})$ in Eq. (68) with that of the classical $H(\mathbf{R})$ in Eq. (17).

B. Structure factor for samples of single size domains

For the finite-size factor in Eq. (68), we now calculate $S(q)$ for samples consisting of domains of a single size. Using Eqs. (26), (45), and (68), we obtain

$$S(q) = \int_0^L dz\; S_1(q,z)S_2(q,z), \tag{69}$$

where

$$S_1(q,z) = 2G_{A1}(0,z)\cos(q_h z)\cos(qz)(L-z), \tag{70}$$

and

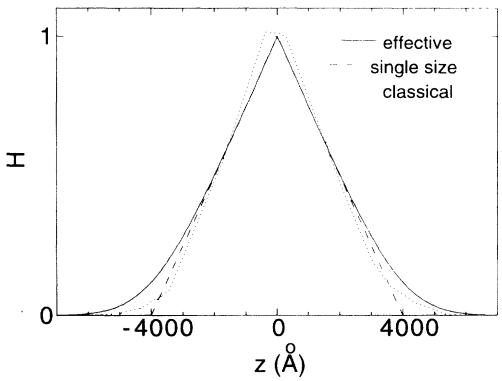

FIG. 8. Comparison of the z variations of the single domain finite-size factor (dashed line) in Eq. (68), the classical (Gaussian) finite-size factor (dotted line) in Eq. (17), and our effective finite-size factor $H_{eff}(z)$ (solid line) from Eq. (82) for $L_0 = 4000$ Å, $\sigma_L = 1200$ Å.

$$S_2(q,z) = \int_0^{L_x}\int_0^{L_y} dxdy\;(L_x-x)(L_y-y) \times e^{-\eta_h r^2/4\lambda z}\frac{4\sin(qr)}{qr}. \tag{71}$$

As we discussed in Sec. III, the rapidly oscillatory factor $\sin(qr)$ determines that the S_2 integral is very insensitive to the values of the integrand in the large r region ($r^2 \gg 4\lambda z$). Therefore we can extend the upper integral limits to ∞, and make $L_x \sim L_y \to L_r$. This means that the specific shapes of the domains are not important to $S(q)$. Then, Eq. (71) yields

$$\begin{aligned} S_2(q,z) &\approx \int_0^\infty r dr\int_0^{\pi/2} d\theta\;(L_r - r\cos\theta)(L_r - r\sin\theta) \times e^{-\eta_h r^2/4\lambda z}\frac{4\sin(qr)}{qr} \\ &= \frac{2}{q}\int_0^\infty dr(\pi L_r^2 - 4rL_r + r^2) \times e^{-\eta_h r^2/4\lambda z}\sin(qr). \end{aligned} \tag{72}$$

We furthermore evaluate Eq. (72) as

$$S_2(q,z) = \frac{16}{q^4}\left[\frac{\pi}{4}(L_r q)^2\zeta_z\;{}_1F_1\left(1,\frac{3}{2},-\zeta_z\right) -\sqrt{\pi}(L_r q)\zeta_z^{3/2}e^{-\zeta_z} +\zeta_z^2\;{}_1F_1\left(3,\frac{3}{2},-\zeta_z\right)\right], \tag{73}$$

where $\zeta_z = \lambda z q^2/\eta_h$. Here we have two large quantities: $L_r q \sim N \gg 1$, and $\zeta_z \sim \lambda z/D^2\eta_h \gg 1$ for $z \gg D$. The asymptotic expansions to the ${}_1F_1$ functions,

$$\begin{aligned} {}_1F_1\left(1,\frac{3}{2},-\zeta_z\right) &\sim \frac{1}{2}\zeta_z^{-1}, \\ {}_1F_1\left(3,\frac{3}{2},-\zeta_z\right) &\sim \frac{4\sqrt{\pi}}{3}\zeta_z^{-3}, \end{aligned} \tag{74}$$

simplify Eq. (73) to

$$\begin{aligned} S_2(q,z) &\approx \frac{2\pi L_r^2}{q^2}\left(1 - 8\pi^{-1/2}(L_r q)^{-1}\zeta_z^{3/2}e^{-\zeta_z} +\frac{32}{3}\pi^{-1/2}(L_r q)^{-2}\zeta_z^{-1}\right) \\ &\approx \frac{2\pi L_r^2}{q^2}, \end{aligned} \tag{75}$$

upon neglecting terms like $e^{-\zeta_z}$ and $(L_r q)^{-2}$. Consequently, Eq. (69) becomes

$$S(q) \approx \int_0^L dz\ S_1(q,z)\ \frac{2\pi L_r^2}{q^2}$$
$$= \frac{2\pi L_r^2}{q^2}\int_0^L dz\ G_{A1}(0,z)(L-z)$$
$$\times [\cos(q-q_h)z+\cos(q+q_h)z]. \quad (76)$$

Next, we neglect the part of the integral resulting from the rapidly oscillating term $\cos(q + q_h)z$, which yields very little intensity. Then, we arrive at

$$S(q) = \frac{2\pi L_r^2}{q^2}\int_0^L dz\ G_{A1}(0,z)(L-z)\cos(q-q_h)z. \quad (77)$$

Equation (77) shows that the structure factor $S(q)$ can be calculated by doing a one-dimensional integral over z. Therefore the amount of calculation is greatly reduced, and an extra effort can be made in developing a more realistic model, as we will show in the next subsection. The parameters a and λ also do not appear in Eq. (77) for the same reasons that they dropped out of Eq. (59) in Sec. V.

Equation (77) can be further simplified by removing two approximations in the preceding development. The first approximation was made to Eq. (67) to obtain a continuous finite-size factor in Eq. (68). The reasons for this approximation were to obtain a continuous finite-size factor H to compare to the classical H_C, and to obtain an integral formula, Eq. (77), for $S(q)$. Retaining the discrete finite-size factor in Eq. (67) yields $S(q)$ in the form of a sum:

$$S(q) = \frac{2\pi L_r^2 N}{q^2}\left[1 + 2\sum_{n=1}^{N}\left(1-\frac{n}{N}\right)\cos(qnD)\right.$$
$$\left.\times G_{A1}(0,nD)\right]. \quad (78)$$

The second approximation was made very early in the derivation by replacing q_z by q_h in Eq. (9), following Caillé's original derivation. This requires that there be a separate formula for each peak, each with its own η_h. This approximation is not, however, critical in our derivation. It is primarily used in Eq. (22) to bring $G(\mathbf{R})$ out of the double integral over $dq_x dq_y$. However, since $G(\mathbf{R})$ varies slowly with q_z, the approximation in Eq. (24) applies and the q_z dependence of $G(\mathbf{R})$ can be replaced by q. Then, Eq. (78) applies to all q. Figure 9 shows the resulting $S(q)$ for the same parameters as in Fig. (7). For comparison, the result of Caillé's approximation $q_z = q_h$ in Eq. 78 is also shown in Fig. (9).

Figure (9) shows the reduction in peak heights $s(q_h)$ that has been emphasized in Figs. 2 and 7. Figure (9) also illustrates the problem of obtaining simple values for the $1/s(h)$ correction factors that occur in Eq. (6). Clearly, $I(h)$ depends both upon the angular range over which the data are integrated and upon whether one subtracts a nonzero baseline. As was noted by Worthington and McIntosh [5], and as we have verified by numerical integration, one can eliminate the correction factor $1/s(h)$

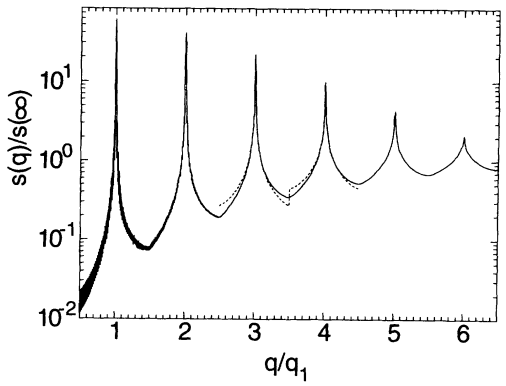

FIG. 9. The reduced structure factor $s(q)/s(\infty)$ given by the term in large square brackets in Eq. (78) for the same parameters as in Fig. 7. The solid curve uses continuous q dependence in the correlation functions and the dashed curve (for $h = 3$ and $h = 4$ only) uses Caillé's approximation.

altogether, i.e., make all $s(h)$ nearly equal, by integrating $s(q)$ from $q = q_h - q_1/2$ to $q = q_h + q_1/2$. To implement this experimentally is not easy, however, because it presumes that there is no other source of scattering between the peaks and that absolute intensity measurements can be made accurately for q values with little scattering. More importantly, it requires that the form factors $F(q)$ do not vary much over these wide angular ranges, which is clearly incorrect. In practice in biophysics, $I(h)$ is measured over narrower q ranges and nonzero baselines are subtracted. Then, the corrections $s(h)$ are closer to the peak heights $s(q_h)$. However, the theory in this paper makes it possible to design more accurate experimental protocols for obtaining the form factors $F(h)$. Specifically, data may be taken near the peaks where they are more reliable and where $F(q)$ does not change rapidly, but over a wide enough q range to obtain the best fitted $s(q)$ near each of the peaks. Then, the theoretical curves for $S(q)$ can be integrated over the same q range as the data to obtain the corrections $s(h)$.

Equation (78) looks very similar to the equations of paracrystalline theory and Eq. (9) of Nallet *et al.* [29]. Because paracrystalline theory uses an *ad hoc* correlation function that decays with distance exponentially instead of as a power law, it gives considerably different peak shapes and peak heights than the theory of Nallet *et al.* and the theory derived in this paper; paracrystalline theory will not be considered further. Equation (9) of [29] is for $S(q_z)$ for oriented samples instead of $S(q)$. Nallet *et al.* point out that, when the Caillé correlation function is used, this gives $|\delta q_z|^{-1+\eta_h}$ power law tails instead of the $|\delta q_z|^{-2+\eta_h}$ tails obtained by Caillé. However, Roux and Safinya [25] had shown that the power law tails for powder samples should go as $|\delta q|^{-1+\eta_h}$. If one assumes infinite domain size in the radial direction, the powder average of their Eq. (9) yields the correct form. We do not use this assumption nor does the difficulty of the incorrect power law tails for oriented samples occur in our derivation of Eq. (78).

It should also be noted that, because all domains have one size, both Eq. (78) and Eq. (9) of Nallet *et al.* give

oscillations in the tails, as can be seen in Fig. 9 for small q values. These oscillations were removed by using a coarse instrumental resolution function by Nallet *et al.* In our theory these oscillations will be removed by averaging over domain sizes as will be shown in the next subsection.

C. Average structure factor for multisize domain samples

In the preceding subsection, we have presented the method of calculating the structure factor $S(q)$ for samples of single size domains. However, for real samples, domains are likely to have a distribution of different sizes. For the domain size distribution function, we choose

$$P(L) \propto e^{-(L-L_0)^2/2\sigma_L^2}, \tag{79}$$

which is essentially a Gaussian distribution except that $P(L) = 0$ for $L < 0$. Next, we use this probability function to average the structure factor in Eq. (77), and obtain the size averaged structure factor as

$$\langle S(q)\rangle = \frac{\frac{2\pi L_r^2}{q^2}\int_0^\infty dLP(L)\int_0^L dzG_{A1}(0,z)(L-z)\cos(q-q_h)z}{\int_0^\infty dLP(L)}$$
$$= \frac{\int_0^\infty dLe^{-(L-L_0)^2/2\sigma_L^2}\int_0^L dzG_{A1}(0,z)(L-z)\cos(q-q_h)z}{\frac{q^2}{2\pi L_r^2}\sqrt{\pi/2}\,\sigma_L[1+\Phi(\zeta_0)]}, \tag{80}$$

where $\zeta_0 = L_0/(\sqrt{2}\sigma_L)$; $\Phi(t) = \frac{2}{\sqrt{\pi}}\int_0^t due^{-u^2}$ is the error function; $G_{A1}(0,z)$ can be obtained from Eq. (45). Notice that $G_{A1}(0,z)$ generally also depends on L.

For a sharp distribution, $\zeta_0 \gg 1$ and $L_0/D \gg 1$, G_{A1} can be replaced by G_{A2} in Eq. (46) which does not depend upon L. Then Eq. (80) becomes

$$\langle S(q)\rangle = \frac{2\pi L_r^2}{q^2}\int_0^\infty dze^{-\eta_h \mathrm{Cin}(\frac{\pi z}{D})}\cos(q-q_h)z\; H_{eff}(z), \tag{81}$$

where

$$H_{eff}(z) = \frac{(\frac{2}{\pi})^{1/2}\sigma_L e^{-(z-L_0)^2/2\sigma_L^2} + (L_0 - z)\left\{1 - \Phi[(z-L_0)/(\sqrt{2}\sigma_L)]\right\}}{1+\Phi(\zeta_0)} \tag{82}$$

is the effective finite-size factor.

Figure 8 shows the new finite-size factor in Eq. (82). Comparison with the z variation of the classical finite-size factor H_C shows that $H_{eff}(z)$ has longer tails and that they are analytically different near $z = 0$. Comparison with the finite-size factor for a single domain in Eq. (68) shows that both have a sharp top at $z = 0$; this is due to strictly periodic structure of the nonfluctuating system in both models (i.e., the systems are perfectly ordered within one domain). Having domains of different sizes does not change the center of the finite-size factor, unless $\sigma_L/L_0 > 1$. In contrast, having multisize domains smears the region near $|z| = L$, when compared to single size domains, as can be seen in Fig. 8.

For the nonfluctuating case ($\eta = 0$) Fig. 10 compares the structure factor $S_0(q)$ from Eq. (80), when H_{eff} is used, to the structure factor from Eq. (27), when H_C is used. Even for this simple case, the two structure factors are different at both the center and the tails. For the central part, the new $S_0(q)$ from Eq. (80) is sharper than the classical $S_0(q)$. The sharpness of the new $S_0(q)$ to a large extent depends on the magnitude of σ_L: larger σ_L yields sharper $S_0(q)$. Therefore, by varying L_0 and σ_L, the width of the top part and bottom part of the new $S_0(q)$ peak can be changed substantially.

Equation (80) is the final formula that describes our modifications to the classical theory. Figure 11 shows the first five orders calculated from Eq. (80) for the same set of parameters with fluctuations as in Figs. 2 and 7. As shown already in Fig. 10 the shapes of these peaks are quite different from those in Fig. 2 and Fig. 7, and this will make a difference in detailed fitting to data.

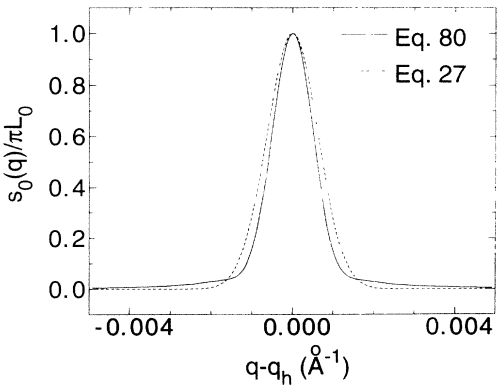

FIG. 10. Comparison of reduced structure factors $s_0(q)/\pi L_0$ calculated, using H_{eff}, from Eq. (80) (solid line) and, using H_C, from Eq. (27) (dashed line). Parameter values are $L_0 = 4000$ Å, $D = 60$ Å, and $\sigma_L = 1200$ Å.

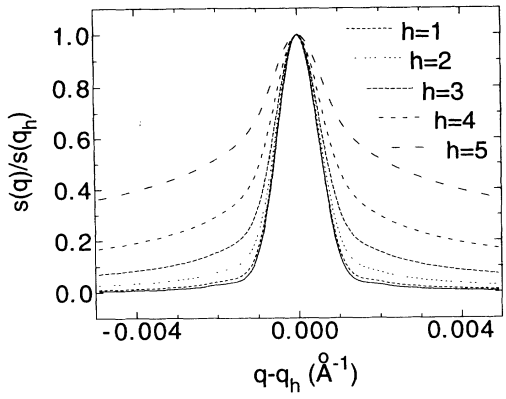

FIG. 11. Normalized reduced structure factor $s(q)/s(q_h)$ for five orders of scattering calculated from Eq. (80). $\eta_1 = 0.03$, $D = 60$ Å, $L_0 = 4000$ Å, $\sigma_L = 1200$ Å. The correction factors $1/s(q_h)$ are 1.14, 1.70, 3.19, 7.18, 17.3 for $h = 1, \ldots, 5$ peaks, respectively.

However, the correction factors $1/s(h) \approx 1/s(q_h)$ that are required to obtain the form factors are similar in size to those obtained in Fig. 7.

VII. CONCLUSIONS

The first result of this paper is to show (see Fig. 2) that the classical scattering theory of Caillé [21] requires very large corrections $1/s(h)$ to the usual calculation of form factors performed routinely in biophysics. This comes about because the scattering at the peaks is very strongly reduced as the scattering order h increases. Although the tails in the scattering also become larger with larger h, with eventual recovery of the intensity if the integration is extended halfway to neighboring peaks [5], there are fundamental difficulties in performing this integration (see Sec. VI). Integrating the intensity over any reasonable angular range does not bring back the lost intensity.

The second result of this paper shows that the very large correction given by the classical Caillé theory is too large, and a more appropriate calculation has been made to obtain better corrections (Fig. 7). The primary reason for the numerical discrepancy was the replacement of the upper limit π/D by infinity in the calculation of the mean square displacements required for the correlation functions in the classical theory [Eq. (11) in Sec. II]. Although this approximation led to a useful closed form solution, we also obtain a closed form approximation that is much more accurate [Eq. (46)]. This improved approximation also yields the power law tails first obtained by the classical theory and amply demonstrated by experiment. Since these power law tails were the primary focus of earlier liquid crystal research [21,23–26], there is no reason for concern for previous results. However, this new result is important for future structural work that requires form factors. In particular, the straightforward application of the classical theory would have resulted in larger errors than those incurred by the standard procedure employed in biophysics that assumes crystalline stacking of the bilayers.

The third result of this paper is the development of an approximation for calculating structure factors for powder samples (Sec. III). This approximation was central to obtaining the other results as well as to obtaining a derivation of a formula proposed by Nallet *et al.* [29] that extends the structure factor calculations to all q values [Eq. (78)].

The fourth result of this paper is the derivation of an alternative finite-size factor [Eq. (82)] to the classical one given by Dutta and Sinha [30]. While the earlier approach is the best one-parameter approximation to the finite-size effect, it does not reproduce the analytic features that one might expect from a reasonable distribution of domain sizes (Fig. 8). Although the distribution of domain sizes is clearly a complicated issue, we believe a Gaussian distribution of domain sizes yields a reasonable approximation for the finite-size factor and we show that the resulting formulas [Eqs. (80) and (81)] are still workable. This modification to the classical theory does not change the form factor corrections significantly, nor does it affect the power law tails. It primarily changes the detailed central line shape. The new finite-size factor provides better fits to our data as will be shown in detail in a subsequent publication. There, it will also be shown how the form factor corrections $1/s(h)$ affect the interpretation of electron density profiles and lipid bilayer structure.

ACKNOWLEDGMENTS

We wish to thank our collaborators, Wenjun Sun, Stephanie Tristram-Nagle, Tom Irving, and Randy Headrick for obtaining the data that have motivated and guided this theoretical development. This research was supported by NIH Grant No. GM44976-04.

APPENDIX

Equation (4) in the text is fairly well known, but it involves some assumptions that involve the fluctuations in the shape of individual bilayers that might be useful to state. The following derivation follows Guinier [37], with the form factors referring to atomic groups consisting of bilayers. The electron density of a single bilayer with midplane at $z = 0$ may be expressed in the minus-fluid description of Worthington *et al.* [4],

$$\rho(\mathbf{R}) = \rho_w + \rho_o(\mathbf{r}, z), \tag{A1}$$

where ρ_w is the electron density of water and $\rho_o(\mathbf{R})$ is zero for $|z|$ greater than $D/2$. The electron density of the nth bilayer in a domain of N bilayers whose average normals are along the z axis can then be written as $\rho_w + \rho_n(\mathbf{r}, z - nD - u_n(\mathbf{r}))$. The nth bilayer is centered at nD on average, but with displacement fluctuations $u_n(\mathbf{r})$. On average $\langle \rho_n \rangle = \langle \rho_o \rangle$ for all lateral positions $\mathbf{r}$, but instantaneous fluctuations require partial form factors $F_n(\mathbf{r}, q_z)$ that depend upon $\mathbf{r}$ and n,

$$F_n(\mathbf{r}, q_z) = \int_{-D/2}^{D/2} dz'\ \rho_n(\mathbf{r}, z')\cos(q_z z'). \quad \text{(A2)}$$

For the domain of N bilayers,

$$\rho(\mathbf{R}) = \rho_w + \sum_n \rho_n(\mathbf{r}, z - nD - u_n(\mathbf{r})). \quad \text{(A3)}$$

Inserting this electron density into the basic x-ray scattering formula,

$$I(\mathbf{q}) = \iint d^3\mathbf{R} d^3\mathbf{R}' \langle e^{i\mathbf{q}\cdot(\mathbf{R}-\mathbf{R}')}\rho(\mathbf{R})\rho(\mathbf{R}')\rangle, \quad \text{(A4)}$$

yields

$$I(\mathbf{q}) = S(\mathbf{q})\ \langle F(\mathbf{q})\rangle|^2 + N[\langle|F(\mathbf{q})|^2\rangle - |\langle F(\mathbf{q})\rangle|^2], \quad \text{(A5)}$$

where $S(\mathbf{q})$ is given by Eq. (7), subject to the following assumptions. (i) It is assumed that fluctuations in $F_n(\mathbf{r}, q_z)$ are uncorrelated with $\mathbf{r}$. This clearly breaks down for small $\mathbf{r}$ due to in-plane structure, but this is significant only for q_r in the wide-angle region. This assumption allows the replacement of the partial form factors in Eq. (A2) with the spatially averaged form factors $F(\mathbf{q})$ in Eq. (A5). (ii) It is assumed that fluctuations in $F_n(\mathbf{r}, q_z)$ are uncorrelated with fluctuations in $u_n(\mathbf{r})$, so that thermal averages of the form factors can be taken independently of the thermal averages involved in the structure factors. This should be a good approximation for long wavelength fluctuations. (iii) It is assumed that fluctuations in the form factors are uncorrelated between different bilayers n and m. Nevertheless, Eq. (A5) still contains a term for fluctuations in the form factors in addition to the term that appears in Eq. (4). This additional term gives broad diffuse scattering that could compete with the scattering from the $S(\mathbf{q})$ structure factor far from the lamellar peaks, but which should play the role of a smooth background for the region near the peaks, which is the region of primary concern in this paper. Ignoring all the effects of fluctuations in the bilayer shape yields Eq. (4) and Eq. (7) which focus upon the fluctuations in the central positions of the bilayers.

[1] A. Tardieu, V. Luzzati, and F. C. Reman, J. Mol. Biol. **75**, 711 (1973).
[2] P. B. Hitchcock, R. Mason, K. M. Thomas, and G. G. Shipley, Proc. Natl. Acad. Sci. USA **71**, 3036 (1974).
[3] M. J. Janiak, D. M. Small, and G. G. Shipley, Biochemistry **15**, 4575 (1976).
[4] C. R. Worthington, G. I. King, and T. J. McIntosh, Biophys. J. **13**, 480 (1974).
[5] C. R. Worthington and T. J. McIntosh, Biophys. J. **14**, 703 (1974).
[6] C. R. Worthington and R. S. Khare, Biophys. J. **23**, 407 (1978).
[7] J. Torbet and M. H. F. Wilkins, J. Theor. Biol. **62**, 447 (1976).
[8] T. J. McIntosh and S. A. Simon, Biochemistry **25**, 4058 (1986).
[9] T. J. McIntosh and S. A. Simon, Biochemistry **25**, 4948 (1986).
[10] M. C. Wiener, R. M. Suter, and J. F. Nagle, Biophys. J. **55**, 315 (1989).
[11] R. P. Rand and V. A. Parsegian, Biochim. Biophys. Acta **988**, 351 (1989).
[12] S. Tristram-Nagle, R. Zhang, R. M. Suter, C. R. Worthington, W.-J. Sun, and J. F. Nagle, Biophys. J. **64**, 1097 (1993).
[13] N. P. Franks and W. R. Lieb, J. Mol. Biol. **133**, 469 (1979).
[14] G. Buldt, H. U. Gally, J. Seelig, and G. Zaccai, J. Mol. Biol. **134**, 673 (1979).
[15] M. C. Wiener and S. H. White, Biophys. J. **59**, 162 (1991).
[16] J. F. Nagle, Biophys. J. **64**, 1110 (1993).
[17] M. A. Davies, W. Hubner, A. Blume, and R. Mendelsohn, Biophys. J. **63**, 1059 (1992).
[18] R. N. A. H. Lewis and R. McElhaney, Biophys. J. **61**, 63 (1992).
[19] J. F. Nagle and D. A. Wilkinson, Biophys. J. **23**, 159 (1978).
[20] J. F. Nagle and M. C. Wiener, Biochim. Biophys. Acta **942**, 1 (1988).
[21] A. Caillé, C. R. Acad. Sci. Ser. B **274**, 891 (1972).
[22] P. G. De Gennes, *The Physics of Liquid Crystals* (Oxford Press, Clarendon, 1974), pp. 284–286.
[23] J. Als-Nielsen, J. D. Litster, R. J. Birgeneau, M. Kaplan, C. R. Safinya, A. Lindegaard-Anderson, and S. Mathiesen, Phys. Rev. B **22**, 312 (1980) .
[24] C. R. Safinya, D. Roux, G. S. Smith, S. K. Sinha, P. Dimon, N. A. Clark, and A.-M. Bellocq, Phys. Rev. Lett. **57**, 2718 (1986).
[25] D. Roux and C. R. Safinya, J. Phys. (Paris) **49**, 307 (1988).
[26] D. C. Wack and W. W. Webb, Phys. Rev. A **40**, 1627 (1989).
[27] R. Hosemann and S. N. Bagchi, *Direct Analysis of Diffraction by Matter* (North-Holland, Amsterdam, 1962).
[28] L. Gunther, Y. Imry, and J. Lajzerowicz, Phys. Rev. A **22**, 1733 (1980).
[29] F. Nallet, R. Laversanne, and D. Roux, J. Phys. II **3**, 487 (1993).
[30] P. Dutta and S. K. Sinha, Phys. Rev. Lett. **47**, 50 (1981).
[31] M. B. Schneider, J. T. Jenkins, and W. W. Webb, Biophys. J. **45**, 891 (1984).
[32] R. M. Servuss, W. Harbich, and W. Helfrich, Biochim. Biophys. Acta **436**, 900 (1976).
[33] V. M. Kaganer, B. I. Ostrovskii, and W. H. de Jeu, Phys. Rev. A **44**, 8158 (1991).
[34] B. E. Warren, *X-ray Diffraction* (Dover Publications, Mineola, N.Y., 1990), pp. 38 and 190.
[35] F. Weling and A. Griffin, Phys. Rev. Lett. **46**, 353 (1981).
[36] B. E. Warren, Phys. Rev. **59**, 693 (1941).
[37] A. Guinier, *X-Ray Diffraction* (Freeman and Co., San Francisco, 1963), Chap. 2, pp. 52 and 53.